Preferred citation: J.D. Redlinger-Pohn, W. Bauer and S. Radl. Fractionation of fibre pulp in a hydrodynamic fractionation device: Influence of Reynolds number and accept flow rate. In **Advances in Pulp and Paper Research, Oxford 2017**, *Trans. of the XVIth Fund. Res. Symp. Oxford, 2017*, (W. Batchelor and D. Söderberg, eds), pp 209–228, FRC, Manchester, 2018. DOI: 10.15376/frc.2017.1.209.

FRACTIONATION OF FIBRE PULP IN A HYDRODYNAMIC FRACTIONATION DEVICE: INFLUENCE OF REYNOLDS NUMBER AND ACCEPT FLOW RATE

Jakob D. Redlinger-Pohn[1], Wolfgang Bauer[2] and Stefan Radl[1]*

[1] Institute of Process and Particle Engineering, Graz University of Technology
[2] Institute of Paper, Pulp and Fibre Technology, Graz University of Technology

ABSTRACT

Fibre fractionation in the Hydrodynamic Fractionation Device (HDF) was studied for changing suspension flow parameters, i.e. different channel Reynolds numbers *Re* and accept flow rates up to 20% of the feed flow rate. The suspension flow behaviour was described using images recorded with a high-speed camera system. Fractionation performance was determined based on mass balances for a variety of length fractions of the pulp. Low Reynolds number flow characterised by $Re = 1300$ led to the formation of a fluid gap between the wall and fibres located at the channel centre. Best fractionation performance was achieved for flow at this Reynolds number: no fibre removal was observed at 10% accept flow rate, and only 1% of the fibres were removed at 20% accept flow rate. A design space was established that highlights the optimum settings for fractionation in an HDF, which are low *Re* and high accept flow rate. Surprisingly, we found a significant increase of fines mass flow rate in the accept upon an increase of the Reynolds number. We speculate that a flow regime-dependent

* Corresponding author: redlinger-pohn@tugraz.at

interaction of fines with the fibres exists in the HDF that critically affects the amount of fines in the fluid gap near the wall.

INTRODUCTION

Fractionation of pulp suspensions and subsequent separate processing of fibre fines, and small fibres promises potential for novel products, precise setting of product and process properties (i.e. dewatering, permeability paper strength), and/or reduction of processing costs. Traditionally pressure screens, i.e. sieves with holes or slots where the pulp is screened by application of a pressure gradient, are applied for the removal of fibre fines, and smaller fibres [1–7]. To avoid sieve blockage, the pulp suspension needs to be continuously stirred, significantly increasing the overall energy demand of pressure screens. Furthermore, a larger amount of fluid is removed from the suspension, especially if only fibre fines are aimed to be removed. Thus, focus was given on alternative processes to fractionate, and/or remove fibre fines and small fibres from pulp suspensions [1, 8–14]: In froth flotation, long fibres are trapped in the flotation froth at comparably high concentration, but contaminated with flotation chemicals [10]. Fractionation in visco-plastic fluids, which also necessitates the addition of chemicals, fractionates suspended material by the potential of particles to apply a force large enough to force a visco-plastic fluid to flow [15]. In hydrocyclones, suspended particles and fibres are fractionated according to their density and shape [8, 12, 16]. Recent improvements of hydrocyclones for pulp fractionation aim on compressing the pulp near the outer region of the cyclone, and remove a fluid layer near the inner region which is enriched with cellulosic fines material [14]. Similarly, length-based fibre fractionation in the so-called Hydrodynamic Fractionation Device (HDF) [11] is achieved by exploiting the natural tendency of longer fibres to form a network [17–19]. For settings of fibre concentration and channel Reynolds number, (long) fibres form a network which is compressed at the channel centre. Consequently, the gap between the network at the channel core and the channel wall is filled with a suspension containing mostly smaller particles or fibres.

In our previous study on the HDF principle, we described the general influence of geometrical parameters (channel height, and channel width), as well as operational parameters (Reynolds number *Re*, accept flow rate, and inlet fibre concentration) on separation performance. Tests were performed with chemical pulp at concentrations yielding crowding number N_{cw} of 9.5, and 47.5. Experimental findings show that geometrical parameters, in the tested range, had no influence on the fractionation quality evaluated by the grade efficiency $T(l_{Fibre})$. The Reynolds number *Re* sets the suspension flow behaviour and thus the amount of gap suspension that forms. Setting the accept flow rate allows control of the frac-

tionation performance. The dependence of the suspension flow behaviour on the channel Reynolds number was investigated via high-speed imaging. However, recorded images in our previous study only allowed qualitative estimation of the *Re* number impact. The fibre concentration in the feed was found to only mildly influence the grade efficiency $T(l_{Fibre})$. For increasing concentration (ranging from 0.1% to 0.5%) a decreasing amount of small fibres and an increasing amount of longer fibres were removed with the accept. We previously speculated that the network strength increased, reducing the mobility of smaller fibres. We note that our previous experiments were performed for relatively low accept flow rates F^+ up to 0.05.

Our more recent visual observations indicate that for certain settings of *Re* a larger accept flow rate could lead to increased fibre fines segregation and thus better fractionation. Therefore, in our present contribution, we aim at the interplay of channel Reynolds number *Re*, and accept flow rate F^+ on the fractionation process. We will perform experiments at *Re* 1300, 2500, and 3700, covering a relevant range of suspension flow regimes. Accept flow rates in this study will be increased up $F^+ = 0.20$. High-speed imaging and image post-processing were improved compared to our previous work, allowing better insight into the fractionation process in our present contribution.

Our contribution is structured as follows: In Chapter 2, we review literature relevant for the fractionation process, namely pulp suspension flow in channels, and length-based fibre separation caused by flow exiting via side channels. In Chapter 3, we present and describe the Hydrodynamic Fractionation Device (HDF). Also, methods for the investigation and the experimental plan are presented. In Chapter 4, we report our results and comment on the findings. We will first present high-speed imaging results, and secondly the measured grade efficiency $T(l_{Fibre})$. Thirdly, we will combine results from both analysis methods. In Chapter 5, we summarise our findings and conclude with an outlook to future studies on hydrodynamic fractionation.

THEORY ON FRACTIONATION IN CHANNEL FLOW

Fibre suspension flow in channels highly depends on the fibres' ability to form a stable and strong network. The strength of the resulting network has to withstand the forces exerted on the network by the ambient fluid. The latter depends on the channel flow rate and can be characterised by the channel Reynolds number *Re* [19–25]. Theory on fibre network formation highlights the importance of mechanical entanglement over attraction by electrostatic forces, or hydrogen-bridge bonding [26–28]. Entanglement is caused by the transport of fibres towards each other, and the subsequent interaction of the fibre bodies and/or fibrils.

Entanglement is more efficient in case of high fibre flexibility, which is directly proportional to fibre length and inversely proportional to fibre diameter/thickness. Kerekes and Schell [26], investigated fibre flocculation and network formation and formulated a dimensionless number, the crowding number N_{CW}, taking above dependencies into consideration:

$$N_{CW} = 5\left[\frac{kg}{m^3}\right]\frac{CL_l^2}{cs}. \tag{1}$$

Here C denotes the fibre mass concentration in percent, L_1 is the length-weighted average fibre length, and cs is the fibre coarseness (i.e., the weight per unit length of fibre). The crowding number was found to describe different fibre interaction regimes: $N_{CW} < 1$: chance of fibre-fibre collision, $1 < N_{CW} < 16$: dilute fibre flow, $16 < N_{CW} < 60$: fibre interaction but no immobilisation, and $N_{CW} > 60$: formation of a strong, coherent structure with immobilisation of fibres. The range $1 < N_{CW} < 60$, predominantly observed in industrial applications, is also termed 'range of forced collision' [29]. Martinez *et al.* [30] showed for fibres settling under gravity, that fibres of different length move freely (i.e. no network restriction) up to $N_{CW} = 16$. For increasing crowding number N_{CW}, first the longer fibres became restricted in a network with the shorter moving freely. At an N_{CW} of 56, all fibres formed a network. The crowding number presenting a change in system behaviour (i.e. $N_{CW} = 16 \pm 4$) was termed 'gelification point'.

Fluid motion in suspension flow exerts forces onto the network. The resulting suspension flow behaviour is consequently a function of the fluid shear and the network strength. Suspension flow behaviour is well documented in the literature [17, 18, 31]. For straight pipe flow the flow regimes (ordered with increasing Reynolds number *Re*) are: (i) fibre plug in direct contact with the wall, (ii) fibre plug with a thin liquid layer (denoted as 'gap suspension') between the wall and the plug, (iii) which thickness increases with the Reynolds number, (iv) becoming eventually turbulent. In the latter state, a relatively high shear stress already acts on the network. Further increase in Reynolds number (v) leads to a dispersion of the plug. While recent studies on fibre suspension flow in channel focused on the fibre plug flow regime, already early studies noted that the gap suspension contains small fibres and fibre fines termed 'crill' [32].

Studies on fibre removal in channel separation flow, i.e. using a side channel to remove fluid from the main channel, where mostly conducted with single fibres freely moving with the suspension and interacting with the wall. The height of the fluid with respect to the wall of the separation channel is directly dependent on the flow rate of the removed fluid (termed accept in what follows). The layer separating the accept from the remaining fluid, i.e. the reject, is termed exit layer.

The probability of fibre removal depends on the fibre wall normal position relative to the exit layer, and the fibres capability to follow the turning flow into the side channel. Theory on single fibre removal is well documented in the literature [9, 33–37], and we applied this knowledge to explain hydrodynamic fractionation in our previous publication [11].

MATERIALS AND METHODS

Hydrodynamic Fractionation Device (HDF)

The Hydrodynamic Fractionation Device is a long channel (i.e. the length is 59 times the channel height) with a separation channel at a position of 52 times the channel height (see Figure 1). The channel height H was set to 15 mm in our present study, while the channel width W was 3 mm. H and W were approximately 3 times, and 0.6 times the length of the longest fibre, respectively. The channel width was chosen to facilitate the image analysis detailed below, since a larger channel width would lead to more fibre-fibre overlaps in projections that are recorded. The HDF is sketched in Figure 1(a), with a magnification of the 3D printed separation channel in Figure 1(b).

The separation channel is orientated backwards, with an upstream angle of 20°, and a downstream angle of 160°. The shape chosen benefited continuous operation by reducing the issue of fibre mat formation. Additionally, we added purge water channels, indicated by blue arrows in Figure 1(b). In this study, only the left

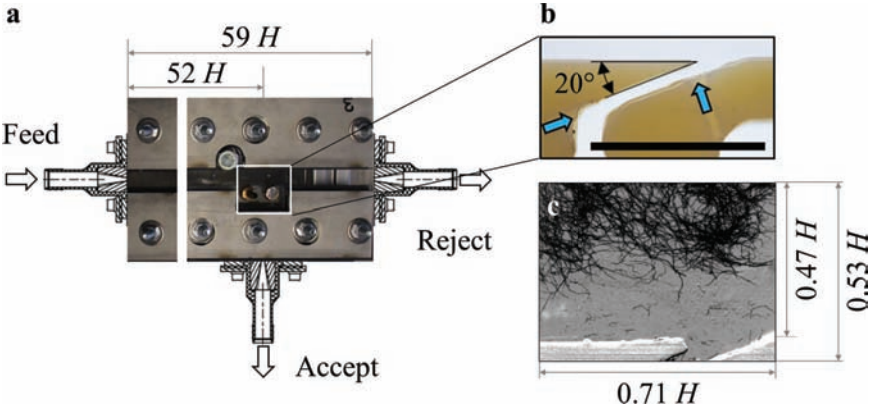

Figure 1. Hydrodynamic fractionation device (a) with magnification on the backwards facing separation channel (b). Purge water channels are indicated in with blue arrows. (c) is a snapshot of the suspension that has been recorded using a high-speed camera.

purge channel was used, at an interval of 120 s, and a purge time of 1 s. The feed flow rate was set by adjusting the geodetic height difference between a feed tank and the height of the reject pipe. The flow rate was determined gravimetrically. The accept flow rate was set by a peristaltic pump (Ismatec ECOLINE VC-280/281, Cole-Parmer GmbH, Germany). Thus, small oscillation of the accept flow rate occurred. Since these oscillations did not significantly alter our results, we only report the mean flow rate in what follows.

Pulp material

Unrefined chemical sulphite pulp, 100% spruce, bleached and washed, provided by Sappi Gratkorn (Austria), was used in this study. Suspensions of 0.1% and 0.2% fibre concentration (only for one set of experiments) were prepared from an initially 17% pulp. Pulp properties were determined from three samples with an L&W Fibre Tester + (Lorentzen & Wettre, Sweden) and are listed in Table 1. The crowding number N_{CW} was calculated using equation 1.

Measurement procedure

Samples were taken from the feed suspension (initial pulp) and the accept flow. The experiment was run for several channel flow-through times before sampling the feed suspension and after re-starting the fractionation process. Sampling was performed three times for each experimental setting.

The fibre concentration C in the samples was determined using thermogravimetric weighing. The fibre length distribution DQ_3, the length-weighted L_1, and volume-weighted L_3 mean fibre length of the samples were determined with an L&W Fibre Tester + according to ISO 16065-2:2014 standard. Fibre length classes for the evaluation were defined as [0.0, 0.2, 0.6, 1.0, 2.0, 3.0, 4.0, 5.5] mm.

The length-selective separation process was quantified by the grade efficiency $T(l_{Fibre})$. The grade efficiency $T(l_{Fibre})$ states the fraction of the feed found in the coarse fraction (i.e. the reject) for a certain fibre length class (l_{Fibre}). Based

Table 1. Pulp properties. Characteristic mean fibre length L_1, and L_3 and fibre coarseness cs.

Length-weighted fibre Length L_1	1.820 mm
Volume-weighted fibre Length L_3	2.447 mm
Fibre coarseness cs	0.174 mg/m
Crowding number N_{CW} for C 0.1%	9.5
Crowding number N_{CW} for C 0.2%	19.0

on our data for the fines fraction (i.e. the accept), the grade efficiency $T(l_{Fibre})$ was calculated from:

$$T\left(l_{Fibre}\right) = 1 - \frac{\dot{m}_{fine}\left(l_{Fibre}\right)}{\dot{m}_{feed}\left(l_{Fibre}\right)} = 1 - \frac{\dot{m}_{fine}\Delta Q_{3,fine}\left(l_{Fibre}\right)}{\dot{m}_{feed}\Delta Q_{3,feed}\left(l_{Fibre}\right)}. \quad (2)$$

Here $\dot{m}$, and $\dot{m}(l_{Fibre})$ state the mass flow and the mass flow per size class, respectively. DQ_3 is the mass or volume-based distribution per size class. The density of the fibre can be assumed equal for all length fractions. Thus the grade efficiency for the process can be formulated as:

$$T\left(l_{fibre}\right) = 1 - \frac{\dot{V}_{accept}C_{accept}\Delta Q_{accept}\left(l_{fibre}\right)}{\dot{V}_{feed}C_{feed}\Delta Q_{feed}\left(l_{fibre}\right)}. \quad (3)$$

The grade efficiency $T(l_{fibre})$ was determined for every experiment, and the mean and standard deviation were calculated and are presented in what follows. The separation efficiency based on the fibre mass in the accept stream f is calculated from the grade efficiency to yield a single value for comparing different cases. f states the mass fraction of fibres from the feed found in the accept flow:

$$f = \frac{\sum \dot{V}_{accept}C_{accept}\Delta Q_{accept}\left(l_{fibre}\right)}{\sum \dot{V}_{feed}C_{feed}\Delta Q_{feed}\left(l_{fibre}\right)}. \quad (4)$$

Image analysis of the fibre suspension flow

Images of the fibre suspension flow at the side channel were recorded using a high-speed camera IDT Os8–S3 (Imaging Solution GmbH, Germany). An exemplary snapshot is presented in Figure 2. Images were taken at a resolution of 1600 × 1200 pixel (width × height), covering an area of 0.71 H times 0.53 H. The suspension height from the wall covered with imaging was 0.47 H. The imaging frequency was adjusted to the flow rate, to take approximately two pictures per time needed for the pulp to pass through the observed length. This procedure guarantees a fair comparison of different cases, i.e. an identical amount of fibres was captured for all experiments. 3,600 images were taken per setting, post-processed and averaged. The image post-processing procedure is illustrated in Figure 2: Raw images (1) are corrected to compensate for fluctuations in the illumination (2). Images are treated using Matlab®'s 'imadjust' command (3), and converted into binary black/white images using a threshold value of 0.4 to

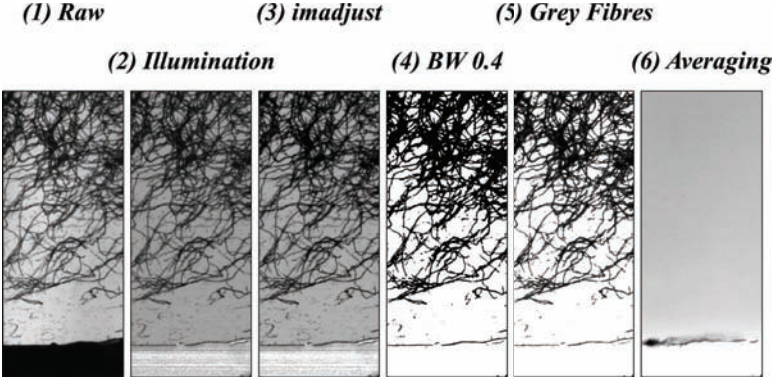

Figure 2. Illustration of the image post-processing routine.

eliminate the grey background (4). Image (3) and image (4) were compared, resulting in image (5), where fibres are presented by their grey value form image (3), with a white background. Using grey scale fibre instead of black/white fibres allows to account for (at least to a first approximation) for overlaying fibres in the projections that were recorded. Finally, the images were averaged resulting in a grey scale map of the fibre intensity (6). The local fibre intensity correlates to the local fibre concentration. However, the intensity additionally depends on the local fibres transparency as well which was not known to us.

Experimental settings

Experiments were conducted for Reynolds numbers Re of 1300, 2500, and 3700 which are within the range of our previous tests [11]. The accept flow rate f^+ was varied from 0.02, to 0.2. Based on the assumption that only the wall-bounded fluid is removed, the accept flow rates equal the exit layer height relative to the height of the flow channel H^*. Experiments were conducted using feed concentrations $C_{feed} = 0.1$ and $C_{feed} = 0.2$. These settings yield a crowding number N_{cw} of 9.5, and 19, respectively.

RESULTS AND DISCUSSION

In what follows we will first analyse the images, and secondly discuss the measured grade efficiency per setting. Thirdly, we will present the origin of the accept fibre mass flow rate in dependence on the wall normal position H^*.

Fibre motion in channel suspension flow

Figure 3 compares snapshots for every case setting (Reynolds number *Re* and feed concentration C_{Feed}), where a region slightly upstream of the side channel is shown. The size of the image section is 0.22 *H* times 0.53 *H*, and the height of the suspension in the image is 0.47 *H*.

Fibre suspension flow at *Re* 1300 leads to a fibre network core in the channel's centre with smaller fibres suspended in the gap suspension. Occasionally, the network at the channel centre was interrupted by flow of either (i) a low concentration suspension, or (ii) a denser fibre plug extending over the full channel height. At *Re* 2500, longer fibres were found suspended in the gap suspension. A fibre network at the channel core contained most of the long fibres. At *Re* 2500, and an increased concentration of C_{Feed} of 0.2% a fibre plug of larger extend was found with a thinner layer of gap suspension. At *Re* 3700, the fibre network extended over the full channel height.

Figure 4 presents the averaged grey values associated with the images presented in Figure 3. Grey scale images with full resolution are presented in the Appendix, Figure 9 to Figure 12.

Figure 3 and Figure 4 show an increase of the fibre concentration (indicated by the grey value) with increasing distance from the wall for *Re* 1300. The distribution

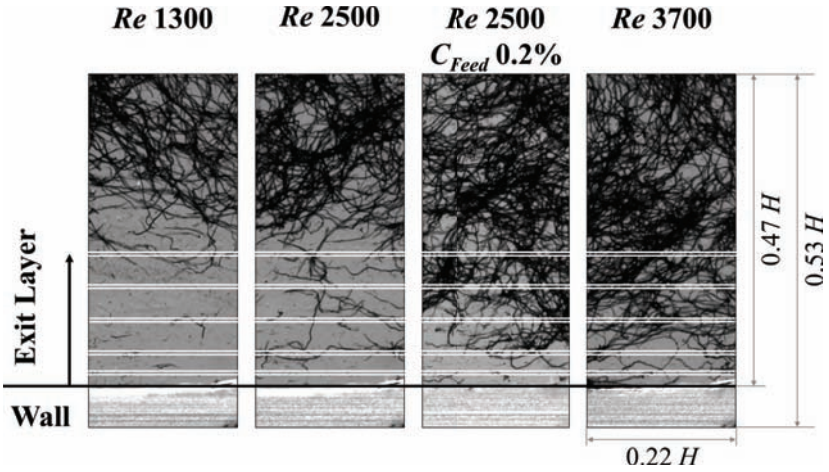

Figure 3. Snapshot of the fibre suspension flow just before the side channel exit for Reynolds numbers *Re* of 1300 (a), 2500 (b), 2500, and 3700 (d). Panel (c) shows the case of 0.2% fibre concentration at *Re* 2500, while all other cases are at a concentration of 0.1%. The black line indicates the channel wall. White lines indicate the averaged exit layer position for f+ of 0.02, 0.05, 0.10, 0.15, and 0.20.

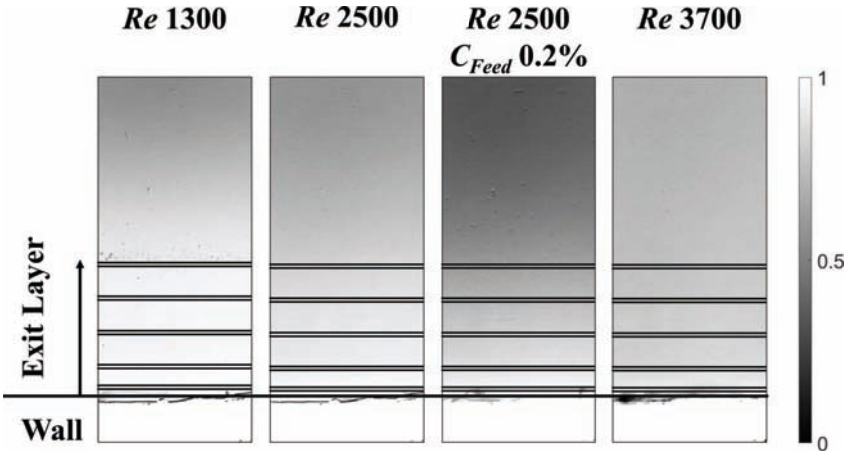

Figure 4. Time-averaged grey scale images associated with the snapshots presented in Figure 3. The wall is indicated by a solid line, while the height of the exit layer is indicated by a black double line. The colour bar states the dimensionless voidage: 1 solid, 0 no solid.

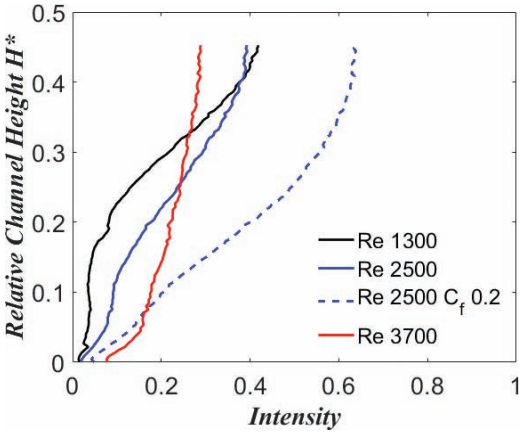

Figure 5. Fibre intensity over the channel height normalised with the channel height H.

of the grey value becomes more even with increasing Reynolds number, as is expected for a larger extent of the fibre plug and/or fluidization of the network. Figure 4(c) and (d) show a significant difference in the grey value distribution, which was not observed in the corresponding snapshots, i.e. Figure 3(c) and (d).

Specifically, the network for *Re* 3700 is looser and fewer fibres were present in this network compared to the case characterised by *Re* 2500 and C_{feed} 0.2%.

Figure 5 presents the averaged fibre intensity over the channel height based on 3,600 recorded images. As can be seen, the intensity for *Re* 1300 is relative low up to a relative channel height H^* of ca. 0.18, increasing steeply thereafter. For *Re* 2500 we find a lower intensity up to H^* of ca. 0.1, with an increase for larger heights which is smaller than for *Re* 1300. These results from the averaged images capture well the difference between the two cases presented in Figure 3. For *Re* 1300 we find mostly medium sized fibres suspended in the suspension gap. For the higher *Re* number of 2500, we still find a network plug at the channel's centre, but with longer fibres suspended in the gap suspension. While Figure 3 only presents one selected time instance, the results from the averaged image analysis shows that those are exemplarily for the suspension, even when the network plug differs in size over time. Doubling the concentration for *Re* 2500 to $C_{Feed} = 0.2\%$ results into similarly shaped profiles, which appear to be simply stretched to larger intensity values. Also, the increase from the channel wall is nearly linear indicating that (i) more of the fibres are found closer to the wall, and (ii) that the network is denser towards the channel centre. For *Re* 3700 we find only a thin region, up to a channel height H^* of approximately 0.02, of low intensity. With increasing height, the increase in the intensity is comparably weak, i.e. the fibre concentration distribution is fairly uniform. This is in line with the description of a 'fluidised state' in literature which is typically observed at high channel Reynolds numbers.

The significance of Figure 5 is that we can clearly determine the formation and position of an interface between a fibre network plug and the so-called gap suspension: for Reynolds numbers *Re* of 1300 and 2500 we find that some fibres are suspended in the gap suspension, while a dense plug of fibres exists near the channel's center. For the channel Reynolds number of 3700 we find the fibres fluidised over the whole channel height.

Fibre removal and grade efficiency

Results for the grade efficiency are presented in Figure 6 for all 4 different cases. The results are within the range of Reynolds number of our previous study [11], i.e. between 1300 and 4000. However, we did increase the accept flow rate in our present study to validate our previous conclusions that were limited to accept flow rates below 0.05.

In general, the results from our present study agree with our previous findings. Figure 6(a) shows the grade efficiency for *Re* 1300. Up to an accept flow rate of 0.05, no fibres longer than 1.5 mm were removed with the accept. Increasing the accept flow rate resulted in a steeper grade efficiency curve, i.e. an improved

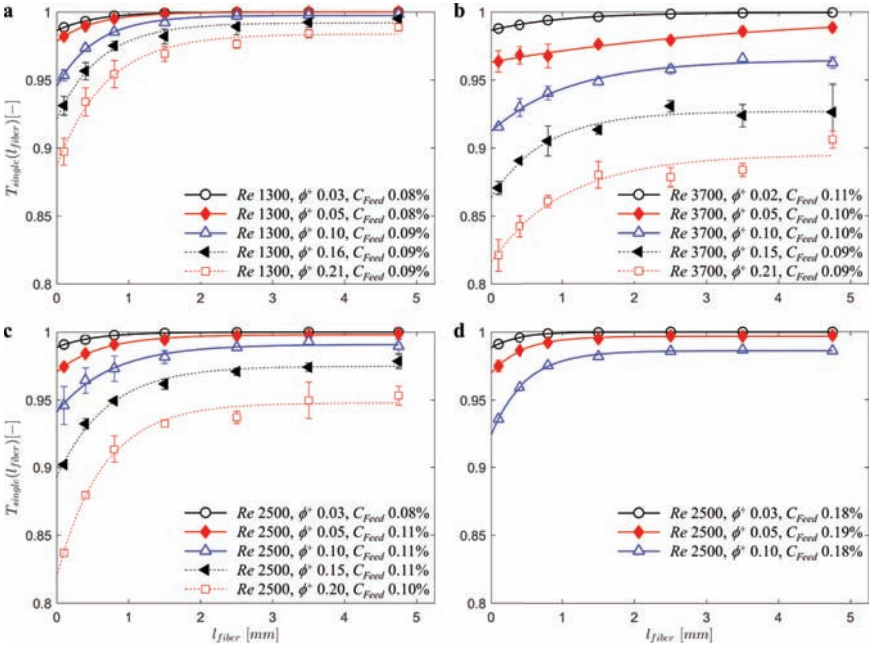

Figure 6. Results for the grade efficiency for different Reynolds numbers and feed concentrations.

fractionation behaviour was observed. However, a minor amount of long fibres, i.e. approximately 1%, was removed with the accept. Results for *Re* 2500 (see Figure 6(c)) are comparable to that collected at *Re* 1300, where no fibre removal was found for accept flow rates up to 0.05. At higher accept flow rates, longer fibres were removed, and fines and fibre removal increased with the accept flow rate. The total removal is significantly higher for *Re* 2500 compared to the case characterised by *Re* 1300. Increasing the Reynolds number to *Re* 3700, leads to a dispersion of the network as shown in Figure 3 to Figure 5. Consequently, a significant amount of long fibres is removed with the accept already at F^+ of 0.05 (see Figure 6(b)). For increasing accept flow rate, both fines and fibres removal increased. No proper fractionation was achieved for *Re* 3700. The impact of fibre concentration is investigated for *Re* 2500 by increasing the concentration from C_{Feed} 0.1% to 0.2% (Figure 6(d)). Fractionation performance, tested up to an accept flow rate of 0.15, was comparable. Slightly higher removal of fines and fibres was observed for C_{Feed} 0.2%, and F^+ of 0.15. The results are consistent with those of our previous findings, were we found increased removal of fibres for higher concentration as well.

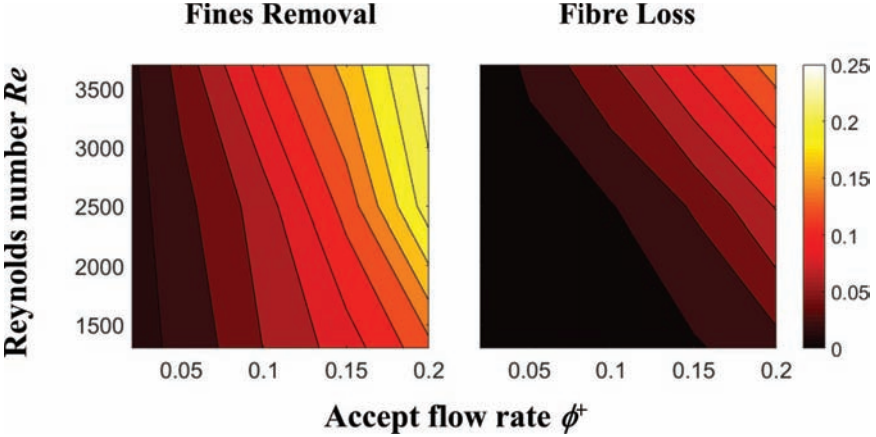

Figure 7. Fines removal and fibre loss characteristics as a function of Reynolds number and accept flow rate.

To detail on the dependence of both, fines and fibre removal on the interplay of Reynolds number *Re* and accept flow rate F^+, we integrated the grade efficiency curve from 0 mm to 0.2 mm, and 0.2 mm to 5 mm and illustrate the fines and fibre removal characteristics in two contour plots shown in Figure 7.

The significance of this representation is that it allows a direct estimation of the effect of operational parameters on the fines removal and fibre loss. The contour lines for the fines removal (see Figure 7, left panel), were nearly vertical, especially for low accept flow rate F^+. This indicates a weak dependency of the fines removal on the Reynolds number *Re*. In contrast, the contour lines for the fibre loss were skewed at nearly 45° inclination (see Figure 7, right panel). Thus, fibre loss was found to depend significantly on the Reynolds number *Re*, a fact that originates from the dependence of the flow structure on *Re*. Best fractionation results were found for an HDF operation in the lower right corner of the panels in Figure 7: high accept flow rate, at low Reynolds number. While Figure 7 allows a direct comparison of fines removal and fibre loss, it needs to be mentioned that such statistical models are only valid in the range of tested parameters. Specifically, the type of pulp and the fibre concentration will affect the data shown in Figure 7.

Accept mass balance per fibre length class

The larger data set acquired, especially larger number of accept flow rates covering a range up to 0.2, allowed the representation of accept fibre mass flow per fibre length. Fines and fibre mass flow in the accept were calculated from the fibre

length distribution in the accept and the total solid mass flow in the accept. Figure 8 shows the cumulative mass flow for 0 mm to 0.2 mm (fines), 0.2 mm to 1 mm (short fibres), and 1 mm to 5 mm (long fibres) fraction relative to the mean mass flow in the channel over the channel height H^*. Comparing the results for increasing *Re* (Figure 8, left to right panel) we find an increase in the mass flow rate for all fibre and fines fractions, i.e. the slope of the curves in Figure 8 decreases with increasing *Re*. The slope of the curve first decreases at higher H^* (*Re* 2500, Figure 8 centre panel), followed by a decrease of the curves' slope over the full height (*Re* 3700, Figure 8 right panel). A slope of 45° represents an equal removal of suspended solids (i.e. fibres or fines) and fluid. We find only for *Re* 3700, and when considering the fines fraction, a nearly equal removal of fluid and fines. Removal of fibres is smaller, which was attributed to (i) the wall-effect for low F^+, and (ii) the turning effect documented in the literature [33] at *Re* 3700. Also, the back facing side channel promotes the fibre exclusion from the accept flow.

Interestingly, the mass flow rate for fines increased with the Reynolds number *Re*. While this is expected for fibres, judging from image analysis (note, we found fibres concentrated at the channel centre) fines were expected to be distributed all over the channel. However, considering the mass flow rate per fibre length suggests that fines were not equally distributed in the channel for lower *Re* and the non-fluidized fibre suspension. We hypothesise that to a certain extend fines, were caught in the network formed by longer fibres concentrated near the channel centre, already for an average crowding number N_{CW} 9.5. Unfortunately, little literature is available that quantifies the degree of fines retardation in fibre flocs and/or networks. For example, Ajersch [38] argued, that fines might be excluded from flocs. Steenberg *et al.* [32] discussed the exclusion of fines from fibre

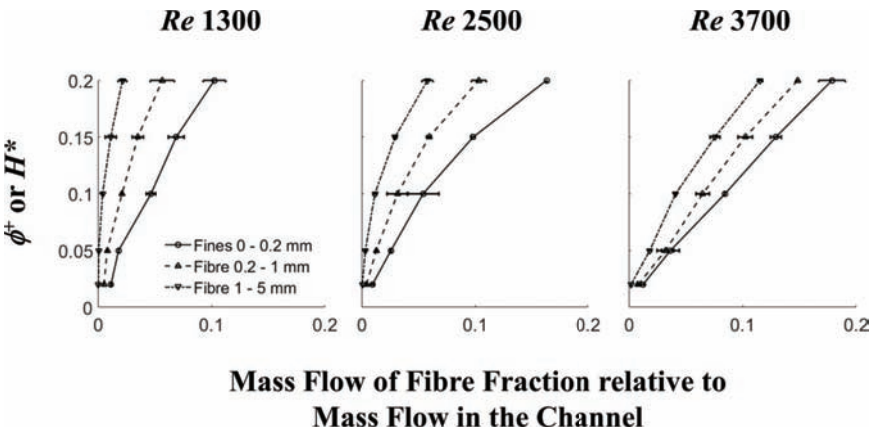

Figure 8. Fines and fibre removal characteristic for different Reynolds numbers, *Re*.

networks. While they discussed differences in the types of fines, they failed to quantify the amount of fines in the fibre network.

CONCLUSIONS

The hydrodynamic fractionation device (HDF) presents a new type of fractionator for length based fibre separation. The fractionation principle was reported in an earlier paper to depend on (i) the effective retention of long fibres in fibre flocs, as well as (ii) the removal of smaller fibres suspended in a wall-bounded fluid layer. In our present contribution, we studied the cross-dependence of the fractionation performance on the suspension's flow regime and the accept flow rate in greater detail to validate these previous conclusions.

We performed optical image analysis with a high-speed camera capturing a section of the channel covering a range from the wall up to 0.47 of the channel height. 3,600 images per case were averaged, and the intensity profile, an indicator of the average mass flow per channel height, was reported. The fibre suspension behaviour in dependence on the Reynolds number *Re* was captured nicely illustrating (i) the extent of the suspension gap for low *Re* flow, (ii) decreasing of this gap with increasing *Re* since fibres are increasingly suspended in the gap suspension, and (iii) finally a fully fluidized suspension, i.e. no gap. Image analysis, compared to grade efficiency measurement, is a relatively fast method allowing a fast screening of suspension flow behaviour and estimations on the fractionation performance for a chosen accept flow rate F^+, and Reynolds number *Re*.

Grade efficiency was determined for a large range of accept flow rates F^+. Best results were observed for low Reynolds numbers, specifically *Re* 1300: up to $F^+ \leq 0.1$, no fibres were removed, and for $F^+ > 0.1$ only 1% of fibres was removed at a fines removal of more than 10%. The results support our hypothesis from our previous study that there is a potential for improving fractionation performance by considering low Reynolds number flows. We compare the fines removal (0 mm to 0.2 mm), and fibre loss (0.2 mm to 5 mm) in a design space of Reynolds number *Re* and accept flow rate F^+. The direct comparison nicely represents the dependence of fibre removal on *Re*. The design space (i) allows a fast decision on the optimal operational parameters of the HDF, and (ii) helps in adjusting *Re* and F^+ to ensure a certain fines removal efficiency or fibre loss. The design space, unfortunately, is only valid in the tested range of parameters and gives no further detail on the separation mechanism.

In a different representation, we plotted the fibre accept mass flow for different length classes, 0 mm to 0.2 mm, 0.2 mm to 1 mm, and 1 mm to 5 mm, as a function of the accept flow rate F^+. Assuming constant fluid removal over the height

via the side channel, the accept flow rate F^+ equals the relative channel height H^*. Surprisingly, we found a dependency of the relative fines mass flow rate on the Reynolds number *Re*. For an increase of the *Re* number from 1300 to 3700 we found nearly double the relative mass flow rate in the accept. We conclude from the result that fines were caught in the network of longer fibres and hence were locked near the channel centre by longer fibres. While we found literature that argued on fines exclusion from flocs [38] and flowing fibre suspensions [32], these studies missed the quantification this phenomenon.

In summary, we verified our hypothesis on the HDF's potential for sharp fractionation by operating it at a suitable Reynolds number *Re*, which results in the formation of a fluid suspension gap with suspended fines. Previous and present studies were performed with 100% spruce sulphite pulp. Future studies will be performed with mixtures of long and short fibre pulp resulting in different network formation and strength. Specifically, we will detail on the types and quality of removed fines for various settings of *Re* and F^+ to shed light on the interaction of fines and fibres in flowing fibre suspensions.

ACKNOWLEDGEMENTS

We gratefully acknowledge the help of Melanie Mayr in establishing the high-speed image post-processing procedure. Furthermore, authors gratefully acknowledge the industrial partners Sappi Gratkorn, Zellstoff Pöls AG, Norske Skog Bruck, and Mondi Frantschach, the Austrian Research Promotion Agency (FFG), COMET, BMVIT, BMWFJ, the Country of Styria, and Carinthia for their financial support of the K-project FLIPPR.

REFERENCES

1. H. Jokinen. Screening and Cleaning of Pulp: A Study to the Parameters Affecting Separation, PhD Thesis, University of Oulu, 2007. http://urn.fi/urn:isbn:9789514284526.
2. M. Karjalainen, A. Ammala, P. Rousu and J. Niinimaki. Fractionation of wheat straw pulp in ultra-fine pressure screening, *Appita J.* **66** (2013) 73–79.
3. S. J. S. Qazi, M. Mohamad, J. A. Olson and D. M. Martinez. Multistage fiber fractionation of softwood chemical pulp through smooth-hole screen cylinders and its effects on paper properties, *TAPPI J.* **14** (2015) 259–267.
4. M. Sloane, P. Kibblewhite, M. Riddell and S. Williams. The Pressure Screen – a Tool for the Modern Fibre Alchemist, in: 60th Appita Annu. Conf. Exhib. Melbourne, Aust. 3–5 April 2006 Proceedings, 2006: pp. 65–73.
5. J. A. Olson. Fibre length fractionation caused by pulp screening, slotted screen plates, J. *Pulp Pap. Sci.* **27** (2001) 255–261.

6. S. Asikainen, A. Fuhrmann and L. Robertsen. Birch pulp fractions for fine paper and board, *Nord. Pulp Pap. Res. J.* **25** (2010) 269–276. doi:10.3183/NPPRJ–2010–25–03-p269–276.
7. S. Mokamati. Effect of Aperture Geometry on the Steady Flow through the Narrow Apertures in a Pulp Screen: Numerical and Experimental Study, PhD Thesis, University of British Columbia, 2007. doi:10.14288/1.0080719.
8. S. Asikainen. Applicability of fractionation of softwood and hardwood kraft pulp and utilisation of the fractions, PhD Thesis, Aalto University, 2015. http://www.vtt.fi/inf/pdf/science/2015/S73.pdf.
9. M. Walmsley and M. Atkins, Comparing Fibre Length Fractionation of a Laboratory Flow Channel to an Industrial Pressure Screen, in: Proc. 57th Appita Annu. Gen. Conf. Exhib., Melbourne, Australia, 2003: pp. 369–376.
10. J. D. Redlinger-Pohn, M. Grabner, P. Zauner and S. Radl, Separation of cellulose fibres from pulp suspension by froth flotation fractionation, *Sep. Purif. Technol*. **169** (2016) 304–313. doi:10.1016/j.seppur.2016.06.004.
11. J. D. Redlinger-Pohn, J. König and S. Radl, Length-Selective Separation of Cellulose Fibres by Hydrodynamic Fractionation, submitted to *Chem. Eng. Res. De*s. (2017).
12. M. Karjalainen, A. Ammala, P. Rousu and J. Niinimaki. Fractionation of wheat straw pulp cells in a hydrocyclone, *Nord. Pulp Pap. Res. J.* **28** (2013) 282–289.
13. A. Karnis. Pulp fractionation by fibre characteristics, *Pap. Ja Puu-Paper Timber.* **79** (1997) 480–488.
14. R. Andersson and H. Vomhoff, Evaluation of a novel hydrocyclone design for pulp fractionation, *Nord. Pulp Pap. Res. J.* **27** (2012) 151–158. doi:10.3183/NPPRJ–2012–27–01-p151–158.
15. A. Madani. Fractionation of Particle Suspensions in a Viscoplastic Fluid: Towards a Novel Process, PhD Thesis, UBC Vancouver, 2011.
16. M. Karjalainen, A. Ämmälä, P. Rousu and J. Niinimäki, Fractionation of epidermal cells from wheat straw pulp by flotation, *TAPPI J.* **14** (2015) 229–235.
17. A. Jäsberg and M. Kataja. New Experimental Results on The Flow Regimes in Closed Channel Flows of Wood Fibre Suspensions, in: 14th Fundam. Res. Symp., Oxford, 2009: pp. 161–180.
18. A. Nikbakht, A. Madani, J. A. Olson and D. M. Martinez, Fibre suspensions in Hagen-Poiseuille flow: Transition from laminar plug flow to turbulence, *J. Nonnewton. Fluid Mech.* **212** (2014) 28–35. doi:10.1016/j.jnnfm.2014.08.006.
19. J. Sha, A. Nikbakht, C. Wang, H. Zhang and J. A. Olson. The effect of concentration and freeness on the yield stress of chemical pulp fibre suspensions, *BioResources* **10** (2015) 4287–4299. doi:10.15376/biores.10.3.4287–4299.
20. R. Eckhart, M. Trimmel and W. Bauer. Experimental Investigation of the Influence of Fibre Morphology on the Interrelation of Flocculation and Network Strength, in: 15th Fundam. Res. Symp., Oxford, 2013: pp. 511–520.
21. B. Norman, K. Moller, R. Ek and G. G. Duffy, Hydrodynamics of Papermaking Fibres in Water Suspensions, in: BPBIF 6th Fund. Res. Symp. Fibre-Water Interact. Papermak., London, 1977: pp. 195–250.

22. C. P. J. Bennington, R. J. Kerekes and J. R. Grace. The yield stress of fibre suspensions, *Can. J. Chem. Eng.* **68** (1990) 748–757. doi:10.1002/cjce.5450680503.
23. B. Chen, D. Tatsumi and T. Matsumoto. Fiber Orientation and flow properties of pulp fiber suspensions under shear flow conditions, *Sen'I Gakkaishi*. **59** (2003) 471–478.
24. M. J. Hourani, Fiber flocculation in pulp suspension flow, Part 1: Theoretical model, *TAPPI J.* **71** (1988) 115–118.
25. F. Lundell, L. D. Söderberg and P. H. Alfredsson. Fluid mechanics of papermaking, *Annu. Rev. Fluid Mech.* **43** (2011) 195–217. doi:10.1146/annurev-fluid–122109–160700.
26. R. J. Kerekes and C. J. Schell. Characterization of fibre floccula tion regimes by a crowding factor, *J. Pulp Pap. Sci.* **18** (1992) 32–38.
27. B. Derakhshandeh, R. J. Kerekes, S. G. Hatzikiriakos and C. P. J. Bennington. Rheology of pulp fibre suspensions: A critical review, *Chem. Eng. Sci.* **66** (2011) 3460–3470. doi:10.1016/j.ces.2011.04.017.
28. R. J. Kerekes. Rheology of fibre suspensions in papermaking: An overview of recent research, *Nord. Pulp Pap. Res. J.* **21** (2006) 598–612. doi:10.3183/NPPRJ–2006–21–05-p598–612.
29. R. M. Soszynski. The Formation and Properties of Coherent Flocs in Fibre Suspension, PhD Thesis, The University of British Columbia, 1987.
30. D. M. Martinez, K. Buckley, S. Jivan, A. Lindström, R. Thiruvengadaswamy, and J. A. Olson, *et al.* Characterizing the Mobility of Papermaking Fibres during Sedimentation, in: 12th Fundam. Res. Symp., 2001: pp. 225–254.
31. A. Nikbakht, A. Madani, J. A. Olson and M. D. Martinez. Observation of the Turbulent Transition of a Fibre Suspension in Hagen-Poiseuille Flow, in: 15th Fundam. Res. Symp., Oxford, 2013: pp. 521–538.
32. B. Steenberg, B. Sandgren and D. Wahren. Studies on pulp crill – Part 1. Suspended fibrils in paper pulp fines, *Sven. Papperstidning*. **63** (1960) 395–397.
33. R. W. Gooding, The Passage of Fibres Through Slots in Pulp Screening, Master Thesis, The University of British Columbia, 1986. doi:10.14288/1.0058886.
34. R. W. Gooding, Flow Resistance of Screen Plate Apertures, PhD Thesis, The University of British Columbia, 1996. doi:10.14288/1.0058507.
35. J. A. Olson, The Effect of Fibre Length on Passage Through Narrow Apertures, PhD Thesis, The University of British Columbia, 1996. doi:10.14288/1.0058501.
36. S. Dong, Modelling of Fiber Motion in Pulp and Paper Equipment, PhD Thesis, The University of British Columbia, 2002. doi:10.14288/1.0103345.
37. A. Kumar. Passage of Fibres Through Screen Apertures, PhD Thesis, The University of British Columbia, 1991. doi:10.14288/1.0059034.
38. M. Ajersch. Mechanisms of Pulp Loss in Flotation Deinking, PhD Thesis, McMaster University, 1997.

APPENDIX

Averaged Grey Images

Figure 9 to Figure 12 present the results from averaging 3,600 images taken from the suspension. The grey value, ranging from 0 to 1, denotes the intensity relating to the fibre concentration. Here, 0 (black) is all fibres, and 1 (white) is no fibre.

Figure 9. *Re* 1300, C_{Feed} 0.1%: Averaged grey image.

Figure 10. *Re* 1300, C_{Feed} 0.1%: Averaged grey image.

Figure 11. *Re* 1300, C_{Feed} 0.1%: Averaged grey image.

Figure 12. *Re* 1300, C_{Feed} 0.1%: Averaged grey image.

Transcription of Discussion

FRACTIONATION OF FIBRE PULP IN A HYDRODYNAMIC FRACTIONATION DEVICE: INFLUENCE OF REYNOLDS NUMBER AND ACCEPT FLOW RATE

Jakob D. Redlinger-Pohn,[1] *Wolfgang Bauer*[2] *and Stefan Radl*[1]

[1] Institute of Process and Particle Engineering, Graz University of Technology
[2] Institute of Paper, Pulp and Fibre Technology, Graz University of Technology

Robert Gooding Advanced Fiber Technologies (AFT)

Thank you for a very nice, very thoughtful, methodical study. I am curious about possible extensions to the work, and if you had thought about the upstream effects? It seems you had a fully-developed flow in your experiments. Have you thought about perhaps using a curved channel upstream of the slot or some sort of enhancement device?

Jakob D. Redlinger-Pohn Graz University of Technology

In short, we are aware of other studies including curved geometries. In particular, a paper from Sweden (Inventia) presents a novel type of hydro cyclone, which is in our opinion similar to the presented Hydrodynamic Fractionation device. In their hydrocyclone, the fibre network is compressed by centrifugal forces at the outer wall, and suspension with fines is removed from the inner wall (Andersson, and Vomhoff, *Nord. Pulp Pap. Res. J.* 27 (2012): 151–158). In a previous study, we also looked into coiled tubes, where we revised current understanding and suggested that fibre network formation has an effect (Redlinger-Pohn et. al., *Int. J. Multiphase Flow* 83 (2016): 239–253). For future work we have thoughts to combine those.

Discussion

Jose Iribarne WestRock

Interesting work. Of course, it reminds me of and I am surprised Robert did not mention it, your geometry is very similar to what happens in a pressure screen on an individual slot, which you can tailor with different wedge wire geometries to get the separation and indeed in industry we use pressure screens as fractionating devices, but at much higher consistencies up to 2% or even higher, and of course we get long fibres in the slot but we get substantially all the fines out. So, can you comment on ultimately that these are very low Reynolds numbers, so that means very large pipes and a lot of energy for the low consistency? How applicable would this be other than for theoretical scientific research?

Jakob D. Redlinger-Pohn

Thank you. That is a question that I often get asked by the person to your left side (Note: Heribert Winter, Sappi Gratkorn GmbH, Austria, one of the project sponsors). I gave a scientific outlook at the end of my talk. As I am working with industry, I can't give a detailed application outlook. The strategy for shifting the hydrodynamic fractionation device to industrial application is up-numbering: fractionators in parallel. Our research work is based on published ideas of particle separation in pressure screen and micro-channel separation. But we found the fibre network formation important. Adding here, we only found recently the work of Duffy (Duffy, *Ann. Trans. Nordic. Rheo. Soc*. 14 (2006)). Thus, we would now state the hydrodynamic fractionation device operates in the *extruded network flow* regime. An interesting point to look at, is the relative pipe diameter compared to the length of the fibres, where the longest fibres might be more important. Also, we one can think of different channel geometries. Also, the rectangular channel, great as it is for optical investigation, is not widely used in industrial applications. In industry one might find pipes instead.

Wenhao Shen South China University of Technology

I think it is very interesting and a very good job and I am wondering about the image analysis software and the fractionation performance evaluation algorithm.

Jakob D. Redlinger-Pohn

The software we used for processing was Matlab. We recorded the images with a high-speed camera: around 3,600 images per case. After image processing with Matlab, we made a movie from the stack of images using ImageJ. For the fractionation, we used an L&W Fibre Tester from Lorentzen & Wettre. We used

the raw data of fibre length and diameter to calculate the grade efficiency. In the evaluation we defined the fibre classes ourselves. Details can be found in the paper.

Wenhao Shen

Okay, so all of these are included in your articles, in the Proceedings?

Jakob D. Redlinger-Pohn

No, the scripts are not included, but the method is described.